

1                   **Rheologic constraints on the upper mantle from five years of**  
2                   **postseismic deformation following the El Mayor-Cucapah**  
3                   **earthquake**

4                   **T. T. Hines<sup>1</sup>, E. A. Hetland<sup>1</sup>**

5                   <sup>1</sup>Department of Earth and Environmental Sciences, University of Michigan, Ann Arbor, Michigan, USA.

6                   **Key Points:**

- 7                   • Transient postseismic deformation can be observed following the El Mayor-Cucapah  
8                   earthquake at epicentral distances of up to 400 km  
9                   • Near-field postseismic deformation exhibits early transience that decays to a sustained  
10                  rate which is elevated above the preseismic trend  
11                  • A Zener or Burgers upper mantle can explain far-field deformation while near-field tran-  
12                  sience can be described with afterslip

13 **Abstract**

14 Five years of postseismic deformation following the Mw7.2 El Mayor-Cucapah earthquake re-  
 15 veals transient deformation that decays back to its pre-earthquake trend after about three years  
 16 at epicentral distances greater than  $\sim 200$  km. At closer distances, the rapid transience decays  
 17 to a sustained rate which exceeds its pre-earthquake trend. We attempt to determine the mech-  
 18 anisms driving this deformation, where we consider afterslip at seismogenic depths and vis-  
 19 coelastic relaxation in the lower crust and upper mantle as candidate mechanisms. We find that  
 20 early, rapid, near-field deformation can be explained with afterslip on the fault that ruptured  
 21 coseismically, while the later, sustained, near-field deformation can be explained with either  
 22 continued afterslip in an effectively elastic lower crust, or lower crustal viscoelastic relaxation  
 23 with a steady-state viscosity of  $\sim 10^{19}$  Pa s. The trend in far-field deformation is best explained  
 24 with a transient viscosity of  $\sim 10^{18}$  Pa s in the upper mantle. We argue that a transient rhe-  
 25 ology in the mantle is preferable over a Maxwell rheology because it better predicts the de-  
 26 cay in postseismic deformation, and also because it does not conflict with the generally higher,  
 27 steady-state viscosities inferred from studies of geophysical processes occurring over longer  
 28 time-scales.

29 **1 Introduction**

30 Ground deformation in the years following a large ( $\gtrsim$ Mw7) earthquake provides insight  
 31 into the mechanical behavior of the crust and upper mantle. It has long been recognized that  
 32 interpretations of postseismic deformation can be ambiguous because multiple postseismic de-  
 33 formation mechanisms can have qualitatively similar surface expressions [e.g. Savage, 1990].  
 34 Owing to the dense geodetic network deployed throughout the 2000s as part of the Plate Bound-  
 35 ary Observatory, the postseismic deformation following the April 4, 2010, Mw7.2 El Mayor-  
 36 Cucapah earthquake in Baja California was observed at more GPS stations than any other earth-  
 37 quake in California to date. With such a large collection of data, we attempt to discern the mech-  
 38 anisms driving postseismic deformation following the El Mayor-Cucapah earthquake, where  
 39 we consider both afterslip and viscoelastic relaxation in the lower crust and upper mantle as  
 40 candidate mechanisms.

41 Previous studies which have modeled postseismic deformation following the El Mayor-  
 42 Cucapah earthquake include Pollitz *et al.* [2012], Gonzalez-Ortega *et al.* [2014], Spinler *et al.*  
 43 [2015], and Rollins *et al.* [2015]. Of these studies, Gonzalez-Ortega *et al.* [2014] and Rollins  
 44 *et al.* [2015] have attempted to describe the postseismic deformation with afterslip in an elas-  
 45 tic half-space. Gonzalez-Ortega *et al.* [2014] described five months of postseismic deforma-  
 46 tion, observed by InSAR and GPS within  $\sim 50$  km of the rupture, with afterslip and contrac-  
 47 tion on the coseismically ruptured fault. Gonzalez-Ortega *et al.* [2014] noted that their preferred  
 48 model underestimated the GPS displacements for stations  $\gtrsim 25$  km from the rupture and sug-  
 49 gested that it could be the result of unmodeled viscoelastic relaxation. Using only continuous  
 50 GPS stations, which are mostly north of the rupture zone, Rollins *et al.* [2015] found that three  
 51 years of postseismic deformation can be adequately explained by afterslip, albeit with an im-  
 52 plausibly large amount of slip inferred on the least constrained, southern-most fault segment.  
 53 Here, we suggest the afterslip inferred by Rollins *et al.* [2015] may have been acting as a proxy  
 54 for distributed relaxation in the upper mantle.

55 Pollitz *et al.* [2012], Rollins *et al.* [2015] and Spinler *et al.* [2015] have explored viscoelas-  
 56 tic relaxation in the lower crust and upper mantle as a potential postseismic deformation mech-  
 57 anism. The rheology of the crust and mantle is largely unknown and so modeling postseis-  
 58 mic deformation with viscoelastic relaxation requires one to assume a rheologic model and  
 59 then find the best fitting rheologic parameters. The inference of these rheologic parameters is  
 60 a computationally expensive non-linear inverse problem which is typically approached with  
 61 a forward modeling grid search method. Consequently, a simplified structure for the Earth must  
 62 be assumed in order to minimize the number of rheologic parameters that need to be estimated.  
 63 For example, it is commonly assumed that the lower crust and upper mantle are homogeneous,

Maxwell viscoelastic layers, which may be too simplistic for postseismic studies [Riva and Govers, 2009; Hines and Hetland, 2013]. To further reduce the dimensions of the model space, it is also necessary to make simplifying assumptions about the nature of afterslip. For example, one can assume a frictional model for afterslip and parametrize afterslip in terms of the unknown rheologic properties of the fault [e.g. Johnson *et al.*, 2009; Johnson and Segall, 2004]. One can also assume that afterslip does not persist for more than a few months and then model the later postseismic deformation assuming it to be the result of only viscoelastic relaxation [e.g. Pollitz *et al.*, 2012; Spinler *et al.*, 2015]. However, postseismic afterslip in similar tectonic settings has been observed to persist for decades following earthquakes [Çakir *et al.*, 2012; Cetin *et al.*, 2014]. Indeed, the preferred viscoelastic model from Pollitz *et al.* [2012] significantly underestimates deformation in the Imperial Valley, which could be indicative of unmodeled continued afterslip. Neglecting to allow for sustained afterslip as a postseismic mechanism could then lead to biased inferences of viscosities.

In this study, we perform a kinematic inversion for fault slip, allowing it to persist throughout the postseismic period, while simultaneously estimating the viscosity of the lower crust and upper mantle. We create an initial model of the fault slip and effective viscosity necessary to describe early postseismic deformation using the method described in Hines and Hetland [2016]. This method utilizes a first-order approximation of surface deformation resulting from viscoelastic relaxation which is only applicable to the early postseismic period. In this case, our initial model describes the first 0.8 years of postseismic deformation following the El Mayor-Cucapah earthquake. We then use the inferred effective viscosity structure from the initial model to create a suite of postseismic models to explain the five years of postseismic data available to date. Of the suite of models tested, we find that postseismic deformation following the El Mayor-Cucapah earthquake can be explained with a combination of afterslip on a fault segment running through the Sierra Cucapah and a Zener rheology in the upper mantle with a transient viscosity that decays from  $6 \times 10^{18}$  Pa s to  $1 \times 10^{18}$  Pa s at 120 km depth.

## 2 Data Processing

We use continuous GPS position time series provided by University Navstar Consortium (UNAVCO) for stations within a 400 km radius about the El Mayor-Cucapah epicenter. We collectively describe the coseismic and postseismic displacements resulting from the El Mayor-Cucapah earthquake as  $u_{\text{post}}(t)$ . We consider the GPS position time series  $u_{\text{obs}}(t)$  to be the combination of  $u_{\text{post}}(t)$ , secular tectonic deformation, annual and semi-annual oscillations, and coseismic offsets from significant earthquakes over the time span of this study. The June 14, 2010, Mw5.8 Ocotillo earthquake and the Brawley swarm, which included an Mw5.5 and an Mw5.4 event on August 26, 2012, (Figure ??) are the only earthquakes that produced noticeable displacements in any of the time series. We treat the displacements resulting from the Brawley swarm as a single event because the daily solutions provided by UNAVCO cannot resolve the separate events. Although the Ocotillo earthquake had its own series of aftershocks [Hauksson *et al.*, 2011], neither the Ocotillo earthquake nor the Brawley swarm produced detectable postseismic deformation. We model displacements resulting from these events with only a Heaviside function,  $H(t)$ , describing the coseismic offsets. We then model  $u_{\text{obs}}(t)$  as

$$u_{\text{obs}}(t) = u_{\text{pred}}(t) + \epsilon, \quad (1)$$

where

$$\begin{aligned} u_{\text{pred}}(t) = & u_{\text{post}}(t)H(t - t_{\text{emc}}) + c_0 + c_1 t + \\ & c_2 \sin(2\pi t) + c_3 \cos(2\pi t) + c_4 \sin(4\pi t) + c_5 \cos(4\pi t) + \\ & c_6 H(t - t_{\text{oc}}) + c_7 H(t - t_{\text{bs}}). \end{aligned} \quad (2)$$

107 In the above equations,  $t_{\text{emc}}$ ,  $t_{\text{oc}}$  and  $t_{\text{bs}}$  are the times of the El Mayor-Cucapah earthquake,  
 108 Ocotillo earthquake, and the Brawley swarm, respectively,  $c_0$  through  $c_7$  are unknown coefficients,  
 109 and  $\epsilon$  is the observation noise. We only estimate jumps associated with the Ocotillo  
 110 earthquake and Brawley swarm for stations within 40 km of their epicenters.

111 Stations which recorded displacements that clearly cannot be described by the aforementioned  
 112 processes are not included in our analysis. This includes stations in the Los Angeles  
 113 basin, where anthropogenic deformation can be larger than the postseismic signal that we are  
 114 trying to estimate [Bawden *et al.*, 2001; Argus *et al.*, 2005]. In order to ensure an accurate es-  
 115 timation of the secular deformation, we only use stations that were installed at least six months  
 116 prior to El Mayor-Cucapah earthquake. Several GPS stations were installed after the El Mayor-  
 117 Cucapah earthquake to improve the spatial resolution of postseismic deformation [Spinler *et al.*,  
 118 2015]. Although it would be possible to subtract secular velocities derived from elastic block  
 119 models [e.g. Meade and Hager, 2005] from velocities recorded at the newly installed stations  
 120 to get an estimate of postseismic velocities, we do not do so here. We use coseismic and post-  
 121 seismic displacements, rather than velocities, in our inverse method described in Section 3. We  
 122 use displacements because estimating velocities from an already noisy displacement time se-  
 123 ries can introduce significant uncertainties depending on exactly how the estimation is done.  
 124 This choice prevents us from using the newly installed stations in Baja California for our anal-  
 125 ysis.

126 The October 16, 1999, Mw7.1 Hector Mine earthquake, which occurred  $\sim$ 270 km north  
 127 of the El Mayor-Cucapah epicenter, produced transient postseismic deformation which we do  
 128 not wish to model, either mechanically or through empirical line fitting. We thus restrict our  
 129 analysis to deformation observed six years after the Hector Mine earthquake, which is when  
 130 postseismic velocities at sites proximal to the Hector Mine epicenter are approximately con-  
 131 stant [Savage and Svare, 2009]. When appraising our model fit in Section 3, we see some sys-  
 132 tematic residuals in the vicinity of the Hector Mine epicenter, which may be the result of er-  
 133 rors in the assumption that the trend in Hector Mine postseismic deformation is linear after  
 134 six years.

135 Studies of postseismic deformation typically assume a parametric form for  $u_{\text{post}}(t)$ , such  
 136 as one with a logarithmic or exponential time dependence [e.g. Savage *et al.*, 2005]. However,  
 137 by assuming a logarithmic or exponential form of  $u_{\text{post}}(t)$  we run the risk of over fitting the  
 138 GPS time series and inferring a non-existent postseismic signal. We therefore do not assume  
 139 any parametric form for  $u_{\text{post}}(t)$  and rather treat it as integrated Brownian motion, so that

$$\dot{u}_{\text{post}}(t) = \sigma^2 \int_0^t w(s) ds, \quad (3)$$

140 where  $w(t)$  is white noise and the variance of  $\dot{u}_{\text{post}}(t)$  increases linearly with time by a fac-  
 141 tor of  $\sigma^2$ . We use a Kalman filtering approach to estimate  $u_{\text{post}}(t)$  and the unknown param-  
 142 eters in eq. (2). In the context of Kalman filtering, our time varying state vector is

$$\mathbf{X}(t) = [u_{\text{post}}(t), \dot{u}_{\text{post}}(t), c_0, \dots, c_7] \quad (4)$$

143 and eq. (2) is the observation function which maps the state vector to the GPS observations.  
 144 We initiate the Kalman filter by assuming a prior estimate of  $\mathbf{X}(t)$  at the first time epoch, de-  
 145 noted  $\mathbf{X}_{1|0}$ , which has a sufficiently large covariance, denoted  $\Sigma_{1|0}$ , to effectively make our  
 146 prior uninformed. For each time epoch  $t_i$ , Bayesian linear regression is used to incorporate  
 147 GPS derived estimates of displacement with our prior estimate of the state  $\mathbf{X}_{i|i-1}$  to form a  
 148 posterior estimate of the state  $\mathbf{X}_{i|i}$ , which has covariance  $\Sigma_{i|i}$ . We then use the posterior es-  
 149 timate of the state at time  $t_i$  to form a prior estimate of the state at time  $t_{i+1}$  through the transi-  
 150 tion function

$$\mathbf{X}_{i+1|i} = \mathbf{F}_{i+1} \mathbf{X}_{i|i} + \delta_{i+1}, \quad (5)$$

151 where

$$\mathbf{F}_{i+1} = \begin{bmatrix} 1 & (t_{i+1} - t_i) & \mathbf{0} \\ 0 & 1 & \mathbf{0} \\ \mathbf{0} & \mathbf{0} & \mathbf{I} \end{bmatrix} \quad (6)$$

152 and  $\delta_{i+1}$  is the process noise, which has zero mean and covariance described by

$$\mathbf{Q}_{i+1} = \sigma^2 \begin{bmatrix} \frac{(t_{i+1} - t_i)^3}{3} & \frac{(t_{i+1} - t_i)^2}{2} & \mathbf{0} \\ \frac{(t_{i+1} - t_i)^2}{2} & (t_{i+1} - t_i) & \mathbf{0} \\ \mathbf{0} & \mathbf{0} & \mathbf{0} \end{bmatrix}. \quad (7)$$

153 The covariance of the new prior state,  $\mathbf{X}_{i+1|i}$ , is then described by

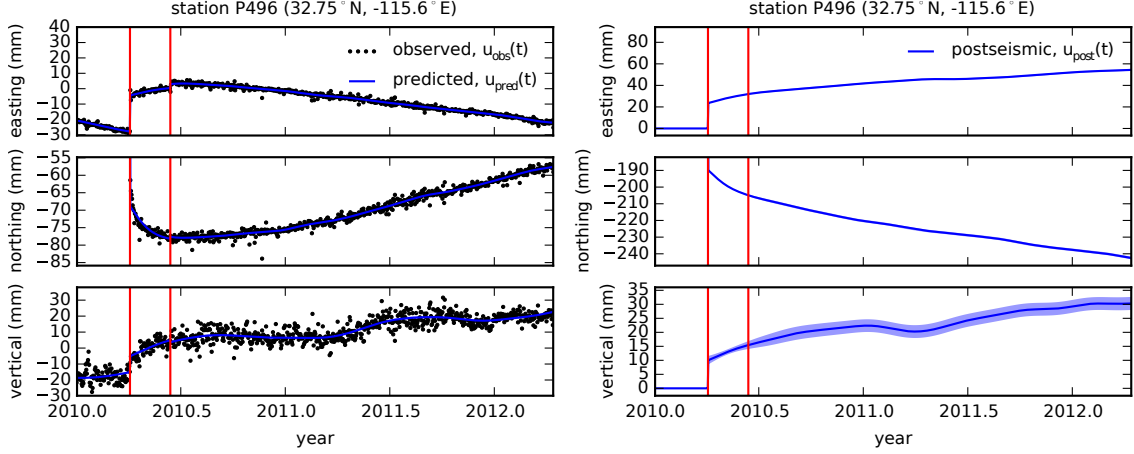
$$\Sigma_{i+1|i} = \mathbf{F}_{i+1} \Sigma_{i|i} \mathbf{F}_{i+1}^T + \mathbf{Q}_{i+1}. \quad (8)$$

154 This process is repeated for each of the  $N$  time epochs at which point we use Rauch-Tung-  
 155 Striebel smoothing [Rauch *et al.*, 1965] to find  $\mathbf{X}_{i|N}$ , which is an estimate of the state at time  
 156  $t_i$  that incorporates GPS observation for all  $N$  time epochs. Our final estimates of  $u_{\text{post}}(t)$   
 157 are used in subsequent analysis, while the remaining components of the state vector are con-  
 158 sidered nuisance parameters. In the interests of computational tractability, we down sample  
 159 our smoothed time series from daily solutions down to weekly solutions.

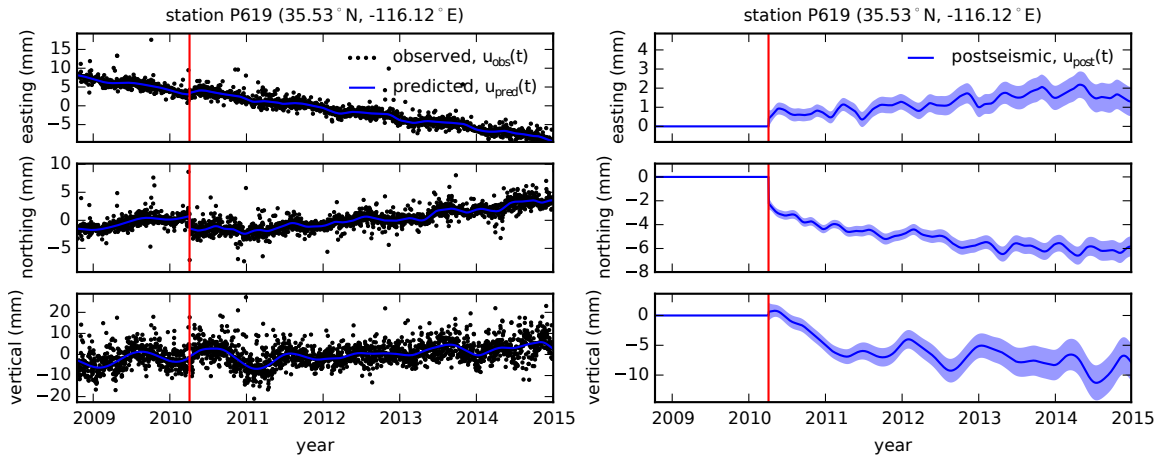
160 The smoothness of  $u_{\text{post}}(t)$  is controlled by the chosen value of  $\sigma^2$ , which describes how  
 161 rapidly we expect postseismic displacements to vary over time. Setting  $\sigma^2$  equal to zero will  
 162 effectively result in modeling  $u_{\text{post}}(t)$  as a straight line which is insufficient to describe the  
 163 expected transient behavior in postseismic deformation. The other end member, where  $\sigma^2$  is  
 164 infinitely large, will result in  $u_{\text{pred}}(t)$  over fitting the data. While one can use a maximum like-  
 165 lihood based approach for picking  $\sigma^2$  [e.g. Segall and Mathews, 1997], we instead take a sub-  
 166 jective approach and choose a value for  $\sigma^2$  that is just large enough to faithfully describe the  
 167 observed deformation at the most near-field station in our study, P496, which exhibits the most  
 168 pronounced rapid changes in velocity. This ensures that  $\sigma^2$  will be sufficiently large so that  
 169 our estimate of  $u_{\text{post}}(t)$  does not smooth out potentially valuable postseismic signal at the re-  
 170 maining stations. We find that using  $\sigma^2 = 0.05 \text{m}^2/\text{yr}^3$  adequately describe all but the first  
 171 week of postseismic deformation at station P496, which gets incorporated into our estimate  
 172 of coseismic displacements (Figure 1). We assume that the first week of deformation is over-  
 173 whelmingly the result of afterslip and this afterslip is lumped into our estimates of coseismic  
 174 slip. Freed *et al.* [2007] noted that postseismic deformation can be observed at distances greater  
 175 than 200 km from the Hector Mine earthquake and, after filtering the time series for stations  
 176 up to 400 km from the El Mayor-Cucapah epicenter, we also clearly see far reaching postseis-  
 177 mic transient deformation (Figure 2).

183 It is important to note that the shown uncertainties in  $u_{\text{post}}(t)$  do not account for the non-  
 184 negligible epistemic uncertainty in eq. (2). For example, we assume a constant rate of secu-  
 185 lar deformation, which appears to be an appropriate approximation for all but perhaps the sta-  
 186 tions closest to the Hector Mine epicenter, as noted above. Also, our model for seasonal de-  
 187 formation in eq. (2) assumes a constant amplitude over time, which means that any yearly vari-  
 188 ability in the climatic conditions could introduce systematic residuals [Davis *et al.*, 2012]. In-  
 189 deed, it would be more appropriate to consider the seasonal amplitudes  $c_2 - c_5$  in eq. (2) as  
 190 stochastic variables [Murray and Segall, 2005]. By using constant seasonal amplitudes, our es-  
 191 timate of  $u_{\text{post}}(t)$  seems to describe some of the unmodeled annual and semi-annual oscilla-  
 192 tions (e.g. Figure 2).

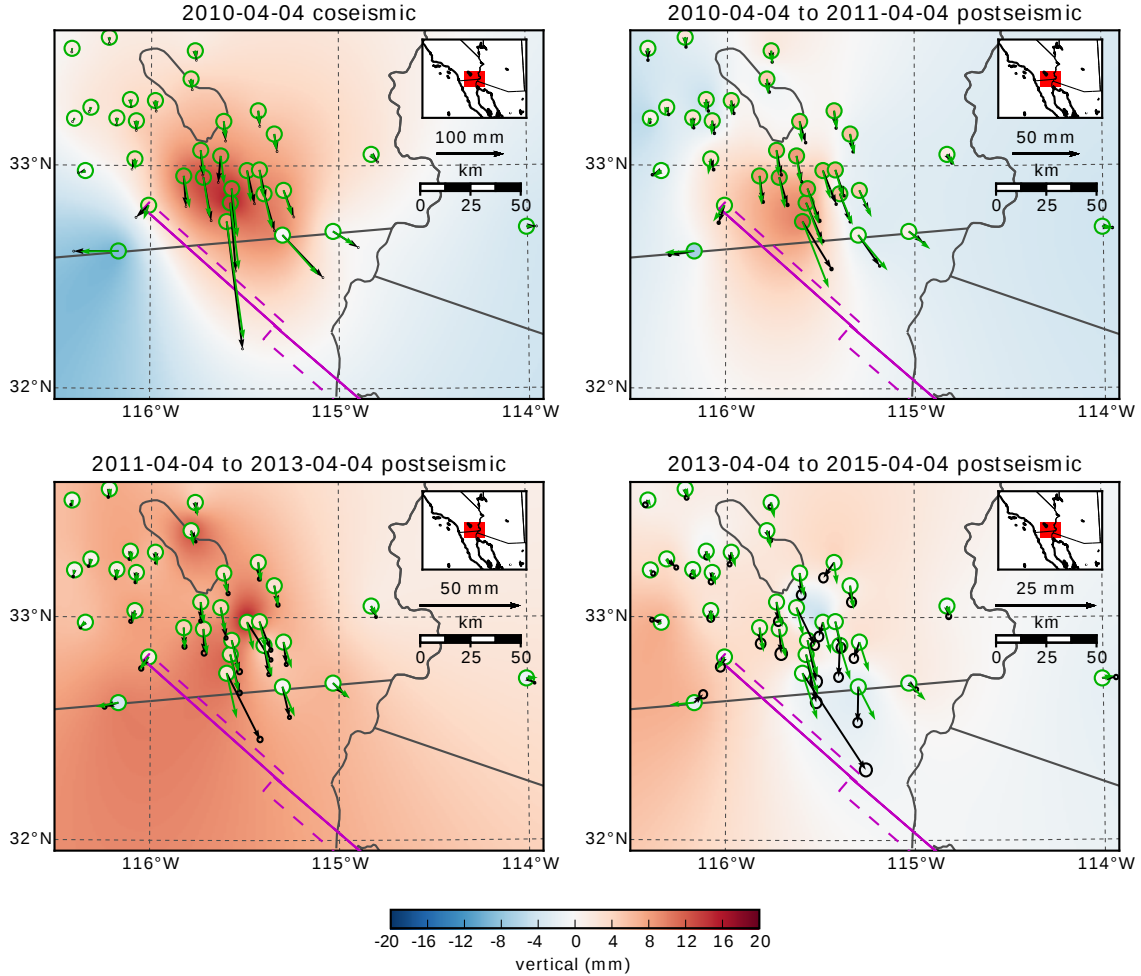
193 We show in Figures 3 and 4 the near and far-field postseismic displacements accumu-  
 194 lated over the time intervals 0-1 years, 1-3 years, and 3-5 years, as well as the coseismic dis-  
 195 placements. Stations at epicentral distances beyond  $\sim 200$  km have an elevated rate of defor-  
 196 mation for the first three years following the earthquake. This far-field deformation has a south-



178 **Figure 1.** Left panels show GPS time series from UNAVCO (black) and the predicted displacement (blue)  
 179 from eq. (2) for a near-field station. Red lines indicate the times of the El Mayor-Cucapah and Ocotillo earth-  
 180 quakes. The right panels show estimated coseismic and postseismic displacements  $u_{\text{post}}$  which are extracted  
 181 from the predicted displacements. The 68% confidence interval is shown in light blue.



182 **Figure 2.** same as Figure 1 but for a far-field station.



207      **Figure 3.** Near-field coseismic and cumulative postseismic displacements over the indicated time periods  
 208      (black) as well as predicted displacements for our preferred model from Section 3.3 (green). Observed verti-  
 209      cal deformation is shown as an interpolated field and predicted vertical displacements are shown within the  
 210      circles at the base of each vector. Note that the interpolant is not well constrained in Mexico where there is no  
 211      data available.

197      ward trend along the direction of the El Mayor-Cucapah P axis and a similar eastward trend  
 198      can be seen in the few far-field stations in Arizona, located along the T axis. After three years,  
 199      the trend in far-field postseismic deformation is barely perceptible. Most far-field stations dis-  
 200      play an initial subsidence for the first year after the El Mayor-Cucapah earthquake followed  
 201      by continued uplift. This trend in vertical deformation can be observed in all three of the quad-  
 202      rants where postseismic data is available, which means that the vertical deformation does not  
 203      exhibit an anti-symmetric quadrant pattern, as would be expected for postseismic processes.  
 204      Although we use vertical deformation in our analysis in Section 3, we do not put an empha-  
 205      sis on trying to describe the vertical deformation as it likely does not have postseismic ori-  
 206      gins.

213      The near-field postseismic deformation is notably sustained when compared to the far-  
 214      field deformation. Namely, the station in this study which is closest to the El Mayor-Cucapah  
 215      epicenter, P496, has been moving at a steady rate of  $\sim 1.5$  cm/yr to the south since about one  
 216      year after the El Mayor-Cucapah earthquake. Vertical postseismic deformation in the near-field  
 217      does display a quadrant pattern which is consistent with the coseismic vertical deformation,

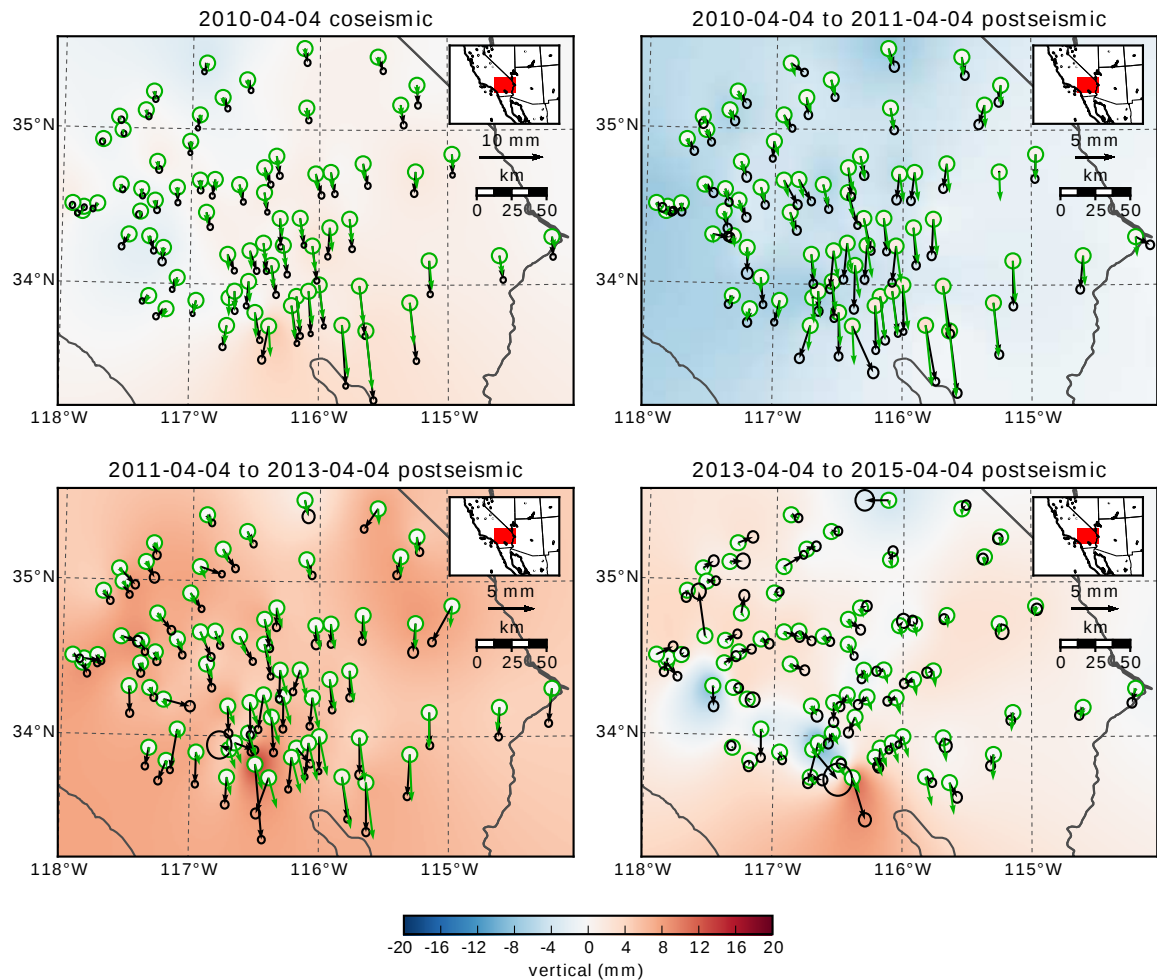


**Figure 4.** Same as Figure 3 but for far-field stations.

212

depth (km)	$\lambda$ (GPa)	$\mu$ (GPa)	$\eta_{\text{eff}}$ ( $10^{18}$ Pa s)	$\mu_k/\mu$
0-5	24.0	24.0	-	-
5-15	35.0	35.0	-	-
15-30	42.0	42.0	44.3	0.0
30-60	61.0	61.0	5.91	0.375
60-90	61.0	61.0	1.99	0.375
90-120	61.0	61.0	1.31	0.375
120-150	61.0	61.0	1.10	0.375
150- $\infty$	61.0	61.0	1.07	0.375

222 **Table 1.** Assumed and estimated material properties.  $\lambda$  and  $\mu$  are assumed known *a priori* and are based  
 223 on the values used for the coseismic model by *Wei et al.* [2011b]. The values for  $\eta_{\text{eff}}$  are estimated in Section  
 224 3.2, and  $\frac{\mu_k}{\mu}$  are the optimal shear moduli ratios found in Section 3.3 for a Zener rheology upper mantle.

218 suggesting that it is resulting from postseismic processes. However, the vertical postseismic  
 219 signal is only apparent for the first year after the earthquake (Figure 3). As with the far-field  
 220 deformation, there is a general trend of uplift in the near-field after about one year.

### 221 3 Postseismic Modeling

222 We seek to find the mechanisms driving five years of postseismic deformation following  
 223 the El Mayor-Cucapah earthquake and we consider afterslip and viscoelastic relaxation as  
 224 candidate mechanisms. Poroelastic rebound has also been used to model postseismic defor-  
 225 mation [e.g. *Jónsson et al.*, 2003]; however, *Gonzalez-Ortega et al.* [2014] found that poroe-  
 226 lastic rebound is unlikely to be a significant contributor to postseismic deformation following  
 227 the El Mayor-Cucapah earthquake. Furthermore, we consider stations which are sufficiently  
 228 far away from the main rupture that poroelastic rebound should be insignificant.

229 We estimate coseismic and time-dependent postseismic fault slip, both of which are as-  
 230 sumed to occur on a fault geometry modified from *Wei et al.* [2011b]. Field studies [*Fletcher*  
 231 *et al.*, 2014] and LIDAR observations [*Oskin et al.*, 2012] have revealed a significantly more  
 232 complicated fault geometry than what was inferred by *Wei et al.* [2011b], especially within the  
 233 Sierra Cucapah. However, we find that a relatively simple coseismic fault geometry based on  
 234 [*Wei et al.*, 2011b] is adequate because most of the stations used in this study are sufficiently  
 235 far from the El Mayor-Cucapah rupture zone that they are insensitive to the details in the fault  
 236 geometry found by *Fletcher et al.* [2014] and *Oskin et al.* [2012]. The fault geometry used in  
 237 this study (Figure ??) consists of the two main fault segments inferred by *Wei et al.* [2011b],  
 238 where the northern segment runs through the Sierra Cucapah up to the US-Mexico border and  
 239 the southern segment is the Indiviso fault which extends down to the Gulf of California. Both  
 240 segments extend from the surface to 15 km depth. We extend the northern segment by 40 km  
 241 to the north-west, motivated by the clustering of aftershocks on the northern tip of the coseis-  
 242 mic rupture zone [*Hauksson et al.*, 2011; *Kroll et al.*, 2013]. This extended fault segment was  
 243 also found to be necessary by *Rollins et al.* [2015] and *Pollitz et al.* [2012] in order to describe  
 244 the postseismic deformation.

#### 245 3.1 Elastic Postseismic Inversion

246 We consider a variety of rheologic models for the lower crust and upper mantle. The  
 247 simplest rheologic model is to consider them to be effectively elastic and isotropic. In such  
 248 case, the rheologic parameters consist of the Lamé parameters,  $\lambda$  and  $\mu$ , which are reasonably  
 249 well known and we use the same values used by *Wei et al.* [2011b] throughout this paper (Ta-  
 250 ble 3). The only unknown is the distribution of fault slip, which can be easily estimated from  
 251 postseismic deformation through linear least squares. Using a subset of the GPS stations con-

sidered in this study, *Rollins et al.* [2015] found that three years of postseismic deformation following the El Mayor-Cucapah earthquake can be explained with afterslip on the coseismic fault plane without requiring any viscoelastic relaxation. We also perform an elastic slip inversion, but we use GPS stations within a larger radius about the El Mayor-Cucapah epicenter (400 km instead of  $\sim$ 200 km). Our forward problem describing predicted postseismic deformation  $u_{\text{pred}}$  in terms of time dependent fault slip,  $s$ , is

$$u_{\text{pred}}(x, t) = \int_F s(\xi, t) g(x, \xi) d\xi, \quad (9)$$

where  $F$  denotes the fault and  $g(x, \xi)$  is the elastic Green's function describing displacement at surface position  $x$  resulting from slip at  $\xi$  on the fault. We estimate coseismic slip and the rate of afterslip at the discrete time intervals, 0.0-0.125, 0.125-0.25, 0.5-1.0, 1.0-2.0, 2.0-3.0, 3.0-4.0, and 4.0-5.0 years after the earthquake. Each fault segment is discretized into roughly 4 km by 4 km patches and we estimate a strike-slip and thrust component of slip for each patch. We impose that the direction of slip and slip rate are within  $45^\circ$  of right-lateral. We also add zeroth-order Tikhonov regularization so that our solution for  $s$  satisfies

$$\min_s \left( \left\| \frac{u_{\text{pred}}(s) - u_{\text{post}}}{\sigma_{\text{post}}} \right\|_2^2 + \lambda_s \|s\|_2^2 \right), \quad (10)$$

where  $\sigma_{\text{post}}$  is the uncertainty on postseismic displacements and  $\lambda_s$  is a penalty parameter which is chosen with a trade-off curve. We use Pylith [Aagaard et al., 2013] to compute the Green's functions for this inversion as well as for the remaining inversions in this paper.

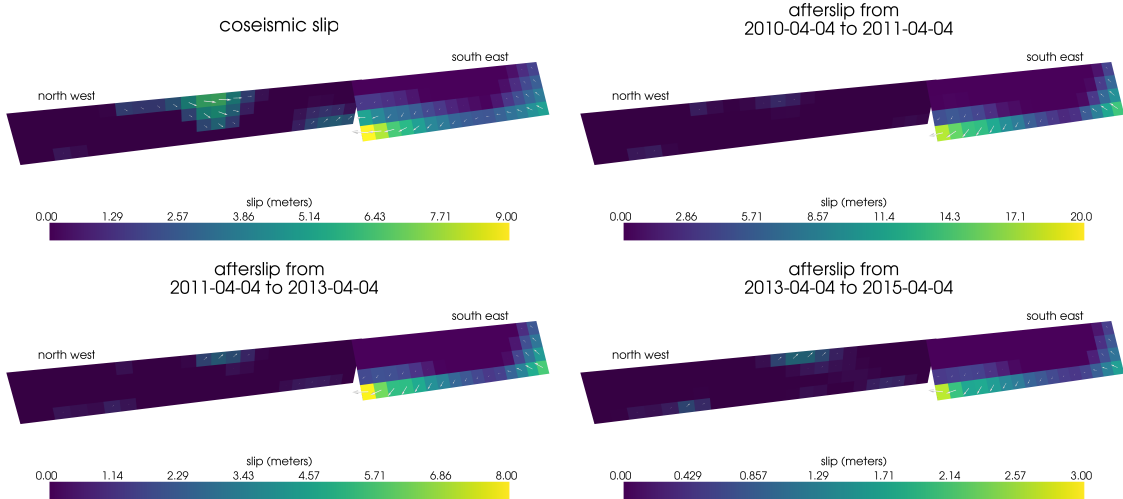
Our coseismic slip and afterslip solutions are shown in Figure 5. As with *Rollins et al.* [2015], we find that a large amount of afterslip on the southern fault segment is required to explain the observations. The potency of our inferred coseismic slip is  $3.2 \times 10^9 \text{ m}^3$ , equivalent to a Mw7.28 earthquake when assuming a shear modulus of 32 GPa. The potency of our inferred cumulative five years of afterslip is  $6.1 \times 10^9 \text{ m}^3$ , equivalent to a Mw7.46 earthquake, which is unrealistically large if we consider afterslip to be driven by coseismically induced stresses. Figure 6 shows the time series for the observed and predicted postseismic displacements at stations along the El Mayor-Cucapah P axis. We show the radial component of displacements with respect to the El Mayor-Cucapah epicenter and we also rescale the displacements so that the difference between the minimum and maximum observed displacements are the same for each station. Our elastic slip model accurately describes near-field postseismic deformation and systematically underestimates postseismic deformation at epicentral distances  $\gtrsim 150 \text{ km}$ . When the fault segments used in the inversion are extended down to 30 km depth, rather than 15 km, the systematic far-field residuals are smaller but remain apparent. Because an elastic model requires an unrealistic amount of afterslip and is unable to predict far-field deformation, we move on to consider viscoelastic models in the next section.

### 3.2 Early Postseismic Inversion

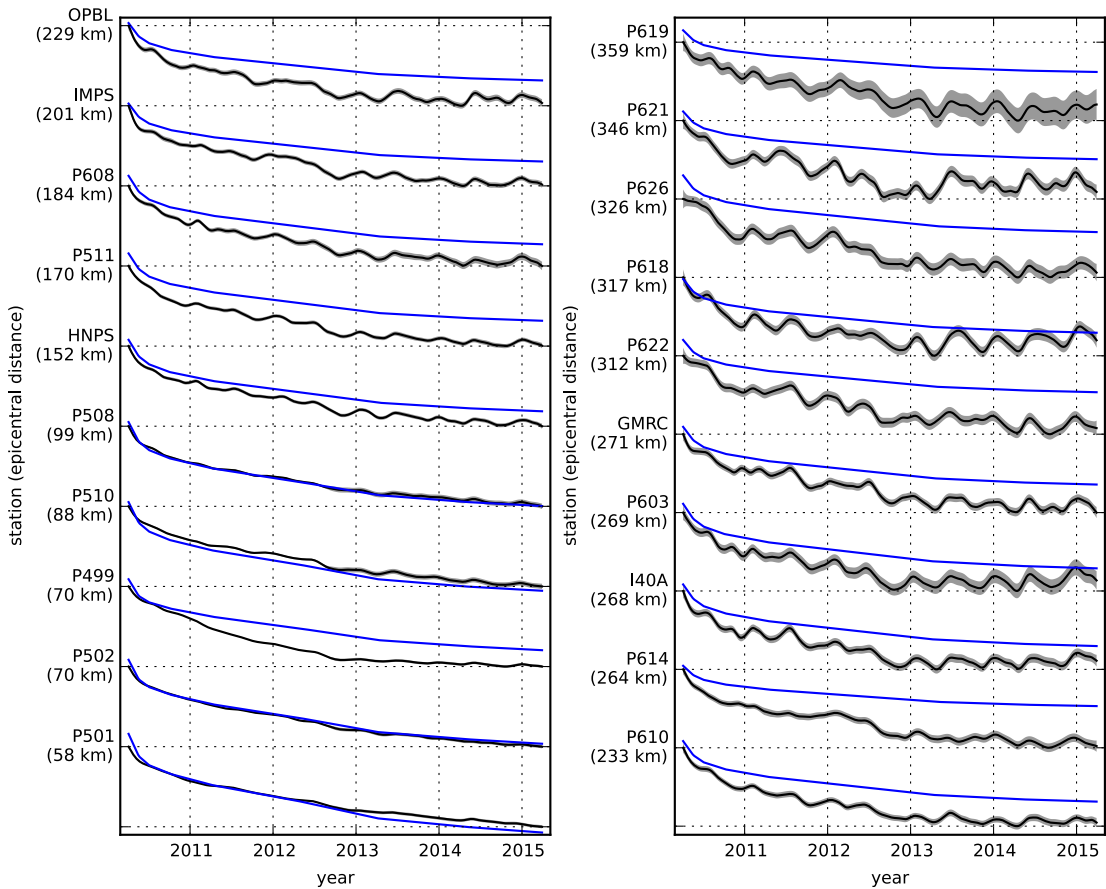
For any linear viscoelastic rheology of the crust and mantle, postseismic displacements resulting from time dependent fault slip can be described as

$$u_{\text{pred}}(x, t) = \int_F s(\xi, t) g(x, \xi) d\xi + \int_0^t \int_F s(\xi, \tau) f(t - \tau, x, \xi) d\xi d\tau, \quad (11)$$

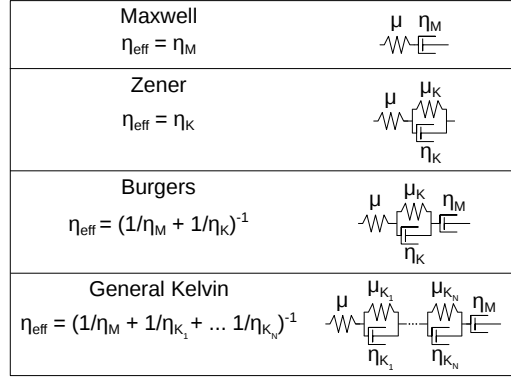
where  $f(t, x, \xi)$  describes the time-dependent velocity at  $x$  resulting from viscoelastic relaxation of stresses induced by slip at  $\xi$ .  $f$  is a function of  $\lambda$ ,  $\mu$ , and any additional rheologic parameters controlling the viscoelastic response, which are generally not well known. Schematic representations of the viscoelastic rheologic models considered in this study are shown in Figure 7. We discuss these rheologic models and their use in geophysical studies in Section 4.



287 **Figure 5.** Coseismic slip and cumulative afterslip over the indicated intervals for the elastic model from  
288 Section 3.1. Color indicates the magnitude of slip while arrows indicate the motion of the hanging wall.



289 **Figure 6.** Scaled radial component of observed postseismic displacements  $u_{\text{obs}}$  (black) and displacements  
290 predicted by the best fitting elastic model  $u_{\text{pred}}$  (blue). Downward motion indicates that the station is moving  
291 toward the El Mayor-Cucapah epicenter. Displacement time series are scaled so that the minimum and max-  
292 imum observed values lie on the grid lines. The 68% confidence interval for the observed displacements are  
293 shown in gray.



302 **Figure 7.** Schematic illustration of the rheologic models considered in this paper as well as their effective  
303 viscosities.

304 In order to greatly simplify the inverse problem, we use the method described in *Hines and Hetland* [2016] to constrain an initial effective viscosity structure from the early postseismic  
305 deformation. Our method utilizes the fact that coseismic stresses throughout the crust and  
306 upper mantle depend on the instantaneous elastic parameters and are independent of the viscoelastic  
307 parameters which we wish to estimate. Immediately following an earthquake, each  
308 parcel will have a strain rate that is proportional to the coseismic stress and inversely proportional  
309 to the parcel's effective viscosity,  $\eta_{\text{eff}}$ . Using one-dimensional viscoelastic models, we  
310 define the effective viscosity as  
311

$$\eta_{\text{eff}} = \left. \frac{\sigma}{\dot{\varepsilon}} \right|_{t=0}, \quad (12)$$

312 where  $\sigma$  is an applied stress at  $t = 0$  and  $\dot{\varepsilon}$  is the resulting strain rate. Figure 7 shows how  
313  $\eta_{\text{eff}}$  relates to the parameters for various linear viscoelastic rheologies. We can deduce that the  
314 initial rate of surface deformation resulting from viscoelastic relaxation is a summation of the  
315 surface deformation resulting from relaxation in each parcel, scaled by the reciprocal of the  
316 parcel's effective viscosity. That is to say

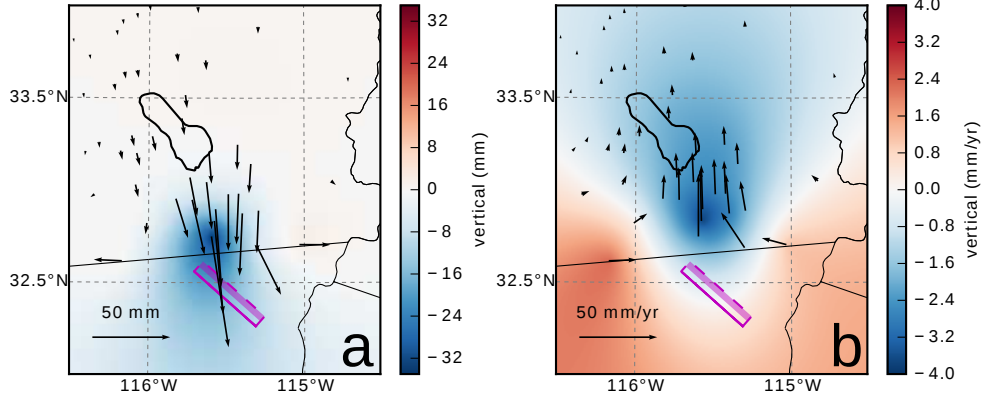
$$f(0, x, \xi) = \int_L \frac{h(x, \xi, \zeta)}{\eta_{\text{eff}}(\zeta)} d\zeta, \quad (13)$$

317 where  $L$  denotes the crust and mantle and  $h(x, \xi, \zeta)$  describes the initial rate of deformation  
318 resulting from viscoelastic relaxation at  $\zeta$  induced by slip at  $\xi$ . We can combine eq. (13) with  
319 eq. (11) to get a first order approximation for early postseismic deformation,

$$u_{\text{pred}}(x, t) \approx \int_F s(\xi, t) g(x, \xi) d\xi + \int_0^t \int_F \int_L \frac{s(\tau, \xi)}{\eta_{\text{eff}}(\zeta)} h(x, \xi, \zeta) d\zeta d\xi d\tau, \quad (14)$$

320 which is valid for as long as the rate of deformation resulting from viscoelastic relaxation is  
321 approximately constant. Although eq. (14) may only be valid for a short portion of the post-  
322 seismic period, its utility becomes apparent when noting that  $g$  and  $h$  are only functions of  
323 the fault geometry and instantaneous elastic properties,  $\lambda$  and  $\mu$ , and thus  $g$  and  $h$  can be com-  
324 puted numerically as a preprocessing step. The forward problem in eq. (14) can then be rapidly  
325 evaluated for any realization of  $s$  and  $\eta_{\text{eff}}$ . This is in contrast to evaluating the full forward  
326 problem, eq. (11), numerically for each realization of  $s$  and the unknown rheologic proper-  
327 ties.

328 Details on how eq. (14) is used to estimate  $s$  and  $\eta_{\text{eff}}$  from postseismic deformation can  
329 be found in *Hines and Hetland* [2016]. A non-linear Kalman filter based inverse method can



358 **Figure 8.** Displacements resulting from fault slip at lower crustal depths (a), and initial velocities resulting  
 359 from subsequent relaxation of a viscoelastic lower crust (b). The fault segment dips  $75^\circ$  to the north-east and  
 360 its surface projection is outlined in magenta. The highlighted area on the fault extends from 15 to 30 km depth  
 361 and indicates where 1 meter of right-lateral slip was imposed. The elastic properties of the crust and mantle  
 362 are the same as in Table 3, and  $\eta_{\text{eff}}$  is  $10^{18}$  Pa s in the lower crust. Vertical displacements are interpolated  
 363 between station locations.

330 also be used to estimate  $s$  and  $\eta_{\text{eff}}$  in a manner akin to Segall and Mathews [1997] or McGuire  
 331 and Segall [2003], in which we would not have to explicitly impose a time dependent parametriza-  
 332 tion of  $s$ . We have thoroughly explored Kalman filter based approaches, but we ultimately pre-  
 333 fer the method described in Hines and Hetland [2016] because of its relative simplicity. More-  
 334 over, we believe the piecewise continuous representation of slip with respect to time to be suf-  
 335 ficiently general for the resolving power of these GPS data.

336 We estimate coseismic slip and afterslip with the same spatial and temporal discretiza-  
 337 tion as in Section 3.1. Simultaneously, we estimate  $\eta_{\text{eff}}$  within six vertically stratified layers  
 338 which have depths ranging from 15–30 km, 30–60 km, 60–90 km, 90–120 km, 120–150 km,  
 339 as well as from 150 km to the bottom of our numerical model domain at 800 km. We again  
 340 restrict fault slip to occur between 0 and 15 km depth, which is done in order to help elim-  
 341 inate inevitable non-uniqueness in the inversion. It has long been recognized that fault slip at  
 342 sufficiently great depths can produce surface deformation that is indistinguishable from vis-  
 343 coelastic relaxation, at least in two-dimensional earthquake models [Savage, 1990]. Addition-  
 344 ally, we note that when simultaneously estimating both afterslip and viscosity in the lower crust,  
 345 the inverse problem becomes particularly ill-posed. This ill-posedness is illustrated in Figure  
 346 8, which shows the displacements resulting from a meter of slip on a fault extending from 15  
 347 to 30 km depth and the initial velocity resulting from subsequent viscoelastic relaxation in the  
 348 lower crust, which is given a viscosity of  $10^{18}$  Pa s. In this demonstration, the viscoelastic re-  
 349 laxation is entirely driven by the fault slip in the lower crust. The horizontal displacements  
 350 from fault slip are in the opposite direction as the displacements resulting from viscoelastic  
 351 relaxation. This means that surface displacements resulting from afterslip at lower crustal depths  
 352 can be cancelled out, at least partially, by a low viscosity lower crust. We eliminate this null  
 353 space by allowing only one mechanism in the lower crust, which we choose to be viscoelas-  
 354 tic relaxation. This is not to say that we do not believe deep afterslip to be a possibility; rather,  
 355 we restrict slip to seismogenic depths as a modeling necessity. Although, it has been noted  
 356 that the pattern of vertical postseismic deformation following the El Mayor-Cucapah earthquake  
 357 indicates that a significant amount of afterslip must be shallow [Rollins et al., 2015].

364 We must determine at which point the early postseismic approximation breaks down, which  
 365 we will denote as  $t_{\text{bd}}$ . As noted, eq. (14) is valid for approximately as long as the rate of de-  
 366 formation resulting from viscoelastic relaxation is approximately constant. We can almost cer-

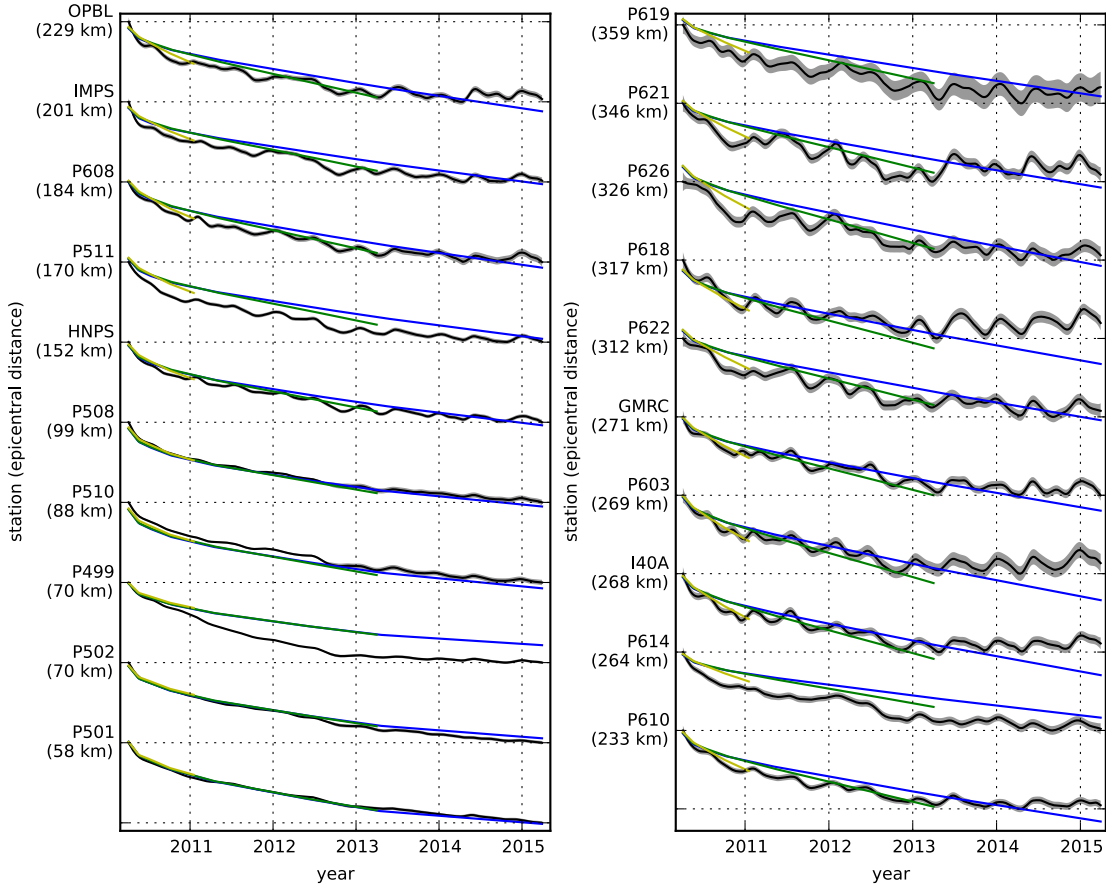


**Figure 9.** Observed postseismic displacements (black) and best fitting predictions of eq. (14) to 5.0 (blue), 3.0 (green), and 0.8 (yellow) years of the postseismic data.

tainly assume that deformation at the most far-field stations, which are  $\sim 400$  km away from the El Mayor-Cucapah epicenter, is the result of viscoelastic relaxation. The approximation should then be valid for as long as a linear trend adequately approximates the far-field deformation. Using this logic, it would appear that  $t_{bd}$  is about one year after the El Mayor-Cucapah earthquake. Another way to determine  $t_{bd}$  is to find the best fitting prediction of eq. (14) to observed deformation using increasing durations of the postseismic time series.  $t_{bd}$  should be the point when eq. (14) is no longer capable of describing the observed deformation without incurring systematic misfits. When using eq. (14) to fit the entire five years of postseismic displacements, we see that the near-field displacements (e.g., station P501) are accurately predicted. When looking at displacements in the far-field (e.g., station P621), we see that eq. (14) overestimates the rate of deformation in the later postseismic period and underestimates the rate of deformation in the early period (Figure 9). Due to the low signal-to-noise ratios for far-field stations, it is difficult to determine at what point eq. (14) is no longer able to predict the observed displacements; however, we settle on  $t_{bd} = 0.8$  years after the earthquake, while acknowledging that the choice is subjective. As noted in Hines and Hetland [2016], overestimating  $t_{bd}$  will result in a bias towards overestimating  $\eta_{eff}$ , while picking a  $t_{bd}$  which is too low will not necessarily result in a biased estimate of  $\eta_{eff}$ , although the uncertainties would be larger. We can then consider inferences of  $\eta_{eff}$  to be an upper bound on the viscosity needed to describe the far-field rate of deformation during the first 0.8 years of postseismic deformation.

We estimate coseismic slip, afterslip, and effective viscosities by solving

$$\min_{s, \eta_{\text{eff}}} \left( \left\| \frac{u_{\text{pred}}(s, \eta_{\text{eff}}) - u_{\text{post}}}{\sigma_{\text{post}}} \right\|_2^2 + \lambda_s \|s\|_2^2 + \lambda_\eta \|\nabla \eta_{\text{eff}}^{-1}\|_2^2 \right), \quad (15)$$

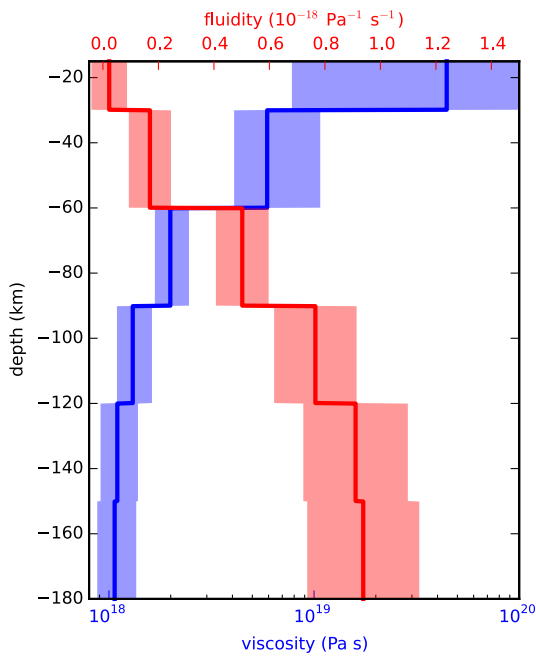
where  $u_{\text{post}}$  consists of the first 0.8 years of postseismic deformation and  $u_{\text{pred}}$  are the predicted displacements from eq. (14). Due to inherent non-uniqueness, we have added zeroth-order Tikhonov regularization to estimates of  $s$  and second-order Tikhonov regularization to estimates of effective fluidity  $\eta_{\text{eff}}^{-1}$ . The degree to which we impose the regularization on slip and fluidity is controlled by the penalty parameters  $\lambda_s$  and  $\lambda_\eta$ , which are chosen with trade-off curves. Our goal here is to get a prior constraint on  $\eta_{\text{eff}}$  to minimize the amount of searching we have to do when describing the postseismic deformation over the full five years, which we do in Section 3.3. Estimates of  $s$  made here will not be used in Section 3.3, and so the motivation behind adding regularization to  $s$  is to ensure that the slip driving viscoelastic relaxation in eq. (14) is sensible.

Our estimated effective viscosities, and corresponding fluidities, are shown in Figure 10. Although fluidity is rarely used in geophysical literature, eq. (13) is linear with respect to fluidity and so the fluidity indicates the amplitude of the viscoelastic signal coming from each layer. We also show the 95% confidence intervals for estimated viscosities and fluidities but we note that the uncertainties tend to be underestimated due to the added regularization [Aster *et al.*, 2011]. A robust feature that we see is that the largest jump in fluidity is at 60 km depth, which is consistent with the range of lithosphere-asthenosphere boundary depths inferred by Lekic *et al.* [2011]. This transitional depth is also consistent with the viscosity structure required to explain far-field postseismic deformation following the Hector Mine earthquake [Freed *et al.*, 2007]. We find that the viscosity below 60 km depth needs to be  $\sim 10^{18}$  Pa s to describe the early rate of postseismic deformation at far-field stations while the lower crust and uppermost mantle need to be relatively stronger. The viscosity of the lower crust is the least well constrained as there is no evidence of relaxation in that layer, meaning that it is effectively elastic over the first 0.8 years after the earthquake.

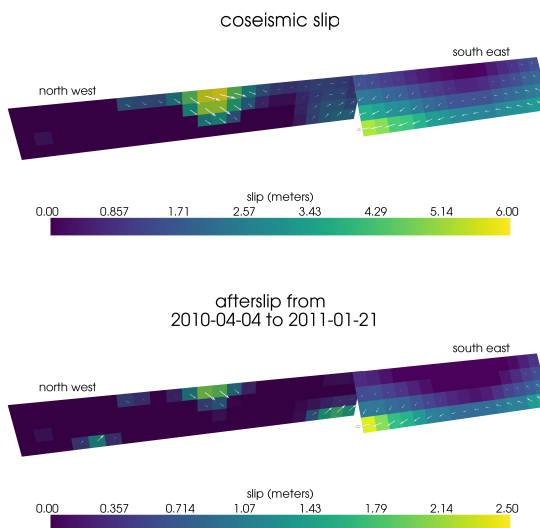
Our initial estimate for coseismic slip and cumulative afterslip over the first 0.8 years after the El Mayor-Cucapah earthquake are shown in Figure 11. Similar to our elastic slip model from Section 3.1, a significant amount of right-lateral and normal coseismic slip is inferred to be on the Sierra Cucapah fault segment. Our coseismic slip solution is consistent with field studies [Fletcher *et al.*, 2014] and the model from Wei *et al.* [2011b]. The potency of inferred coseismic slip is  $3.3 \times 10^9$  m<sup>3</sup>, which is also about the same as that inferred from Section 3.1. The present inference of afterslip on the Indiviso fault is significantly less than what was found in the Section 3.1 where we did not account for viscoelasticity. When fault slip is simultaneously estimated with viscosity, the potency of inferred afterslip over the first 0.8 years after the earthquake is  $0.85 \times 10^9$  m<sup>3</sup>, compared to  $3.5 \times 10^9$  m<sup>3</sup> when we assume the crust and upper mantle are elastic. The significant amount of afterslip inferred on the Indiviso fault seems to be compensating for unmodeled viscoelastic relaxation at depths greater than 60 km. The fact that there is still an appreciable amount of afterslip inferred on the Indiviso fault raises the question of whether it is compensating for viscoelastic relaxation that is more localized than what we allow for since we only estimate depth dependent variations in viscosity.

### 3.3 Full Postseismic Inversion

In the previous section, we used the inverse method from Hines and Hetland [2016] to constrain the effective viscosity structure required to explain the first 0.8 years of postseismic deformation. In this section, we use these effective viscosities as a prior constraint when searching for models which are capable of describing the available five years of postseismic data, where our forward problem is now eq. (11) rather than the approximation given by eq. (14). We perform a series of fault slip inversions assuming a variety of rheologies for the lower crust and upper mantle which are consistent with our findings from Section 3.2. We appraise each model using the mean chi-squared value,



414      **Figure 10.** Effective viscosities and associated fluidities inferred by fitting eq. (14) to the first 0.8 years of  
 415      postseismic displacements. 95% confidence intervals, estimated from bootstrapping, are indicated by color  
 416      fields.



432      **Figure 11.** Coseismic slip and afterslip inferred by fitting eq. (14) to the first 0.8 years of postseismic  
 433      displacements.

$$\bar{\chi}^2 = \frac{1}{N} \left\| \frac{u_{\text{pred}} - u_{\text{obs}}}{\sigma_{\text{obs}}} \right\|_2^2, \quad (16)$$

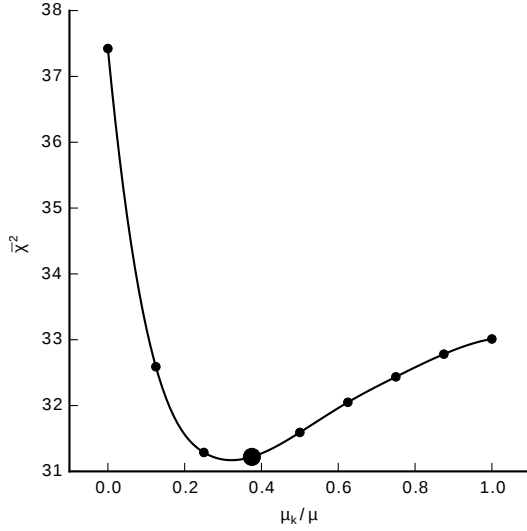
443 where  $N$  is the number of observations.

444 We first assume that the crust and mantle can be described with a Maxwell rheology,  
 445 and we set the steady-state viscosity  $\eta_M$  equal to our inference of  $\eta_{\text{eff}}$ . We compute  $f$  and  $g$   
 446 from eq. (11) using Pylith, and we use the same spatial and temporal discretization of  $s$  as  
 447 in Sections 3.1 and 3.2. We estimate  $s$  using linear least squares and find a misfit of  $\bar{\chi}^2 =$   
 448 37.4. For comparison,  $\bar{\chi}^2 = 35.3$  for the elastic model from Section 3.1. The Maxwell vis-  
 449 coelastic model has a larger misfit because it tends to overestimate the rate of deformation af-  
 450 ter about three years (Figure 13). Since our initial estimates of  $\eta_{\text{eff}}$  may be biased towards over-  
 451 estimating viscosities, we have also performed the slip inversion where we use uniformly lower  
 452 viscosities in the crust and mantle. However, decreasing the viscosity only increases the mis-  
 453 fit. Although, the viscosities used here are consistent with the successful Maxwell viscoelas-  
 454 tic models found by *Rollins et al.* [2015] and *Spinler et al.* [2015], which had mantle viscosi-  
 455 ties on the order of  $10^{18}$  Pa s and relatively higher lower crustal viscosities, we find that such  
 456 a model is incapable of describing the entire postseismic time series. *Pollitz et al.* [2001] sim-  
 457 ilarly recognized this deficiency in a Maxwell rheology, which then motivated their exploration  
 458 of a Burgers rheology upper mantle [*Pollitz*, 2003].

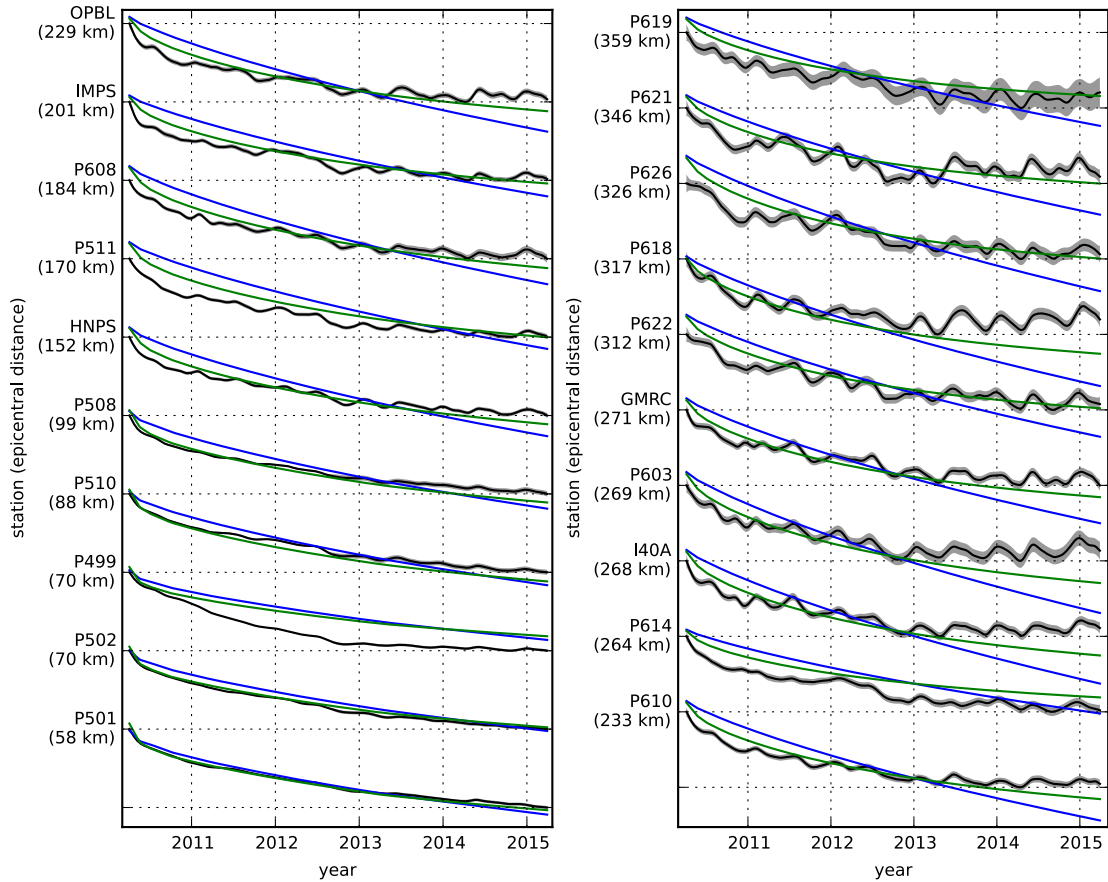
459 Instead of exploring a Burgers rheology mantle, which introduces two new parameters  
 460 that need to be estimated, the transient viscosity  $\eta_K$  and transient shear modulus  $\mu_K$ , we first  
 461 consider a Zener rheology for the mantle, which only introduces one additional unknown pa-  
 462 rameter,  $\mu_K$ . We assume that the lower crust still has a Maxwell rheology. The steady-state  
 463 viscosity in the crust and the transient viscosity in the mantle are set equal to the inferred ef-  
 464 fective viscosities. We then estimate the ratio of shear moduli  $\frac{\mu_K}{\mu}$ . We compute nine differ-  
 465 ent sets of Green's functions,  $f$  and  $g$ , where we assume values of  $\frac{\mu_K}{\mu}$  ranging from 0 to 1.  
 466 The former being a degenerate case where the Zener model reduces to the above Maxwell model.  
 467 We estimate coseismic slip and afterslip for each realization of  $\frac{\mu_K}{\mu}$ . The shear moduli ratio  
 468 that yields the best prediction to the observed postseismic displacements is found to be 0.375  
 469 which produces a misfit of  $\bar{\chi}^2 = 31.2$  (Figure 12). The improvement in the Zener model over  
 470 the Maxwell model can be clearly seen in the fit to the far-field data (Figure 13). The Zener  
 471 model does a significantly better job at explaining the transient rate of far-field deformation  
 472 throughout the five years.

480 Because we are able to adequately describe the available five years of postseismic de-  
 481 formation with a Zener model, we do not find it necessary to explore the parameter space for  
 482 a more complicated Burgers rheology. However, since the Zener model is a Burgers model with  
 483 an infinite steady-state viscosity, we can conclude that any Burgers rheology that has a tran-  
 484 sient viscosity consistent with that found in Section 3.2 and a steady-state viscosity  $\gtrsim 10^{20}$   
 485 Pa s, which is effectively infinite on the time scale of five years, would also be able to sat-  
 486 isfactorily describe the observable postseismic deformation.

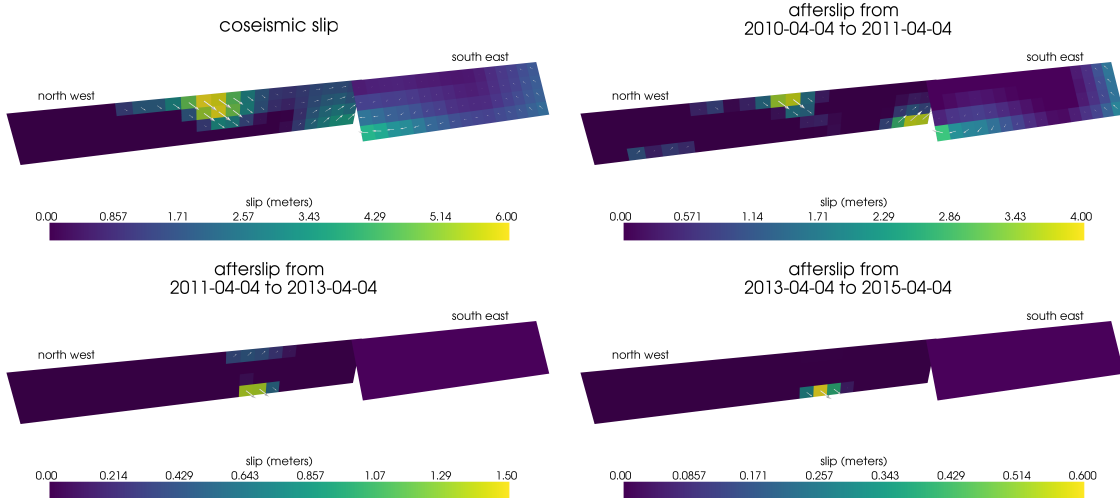
487 The regularized inference of coseismic slip and afterslip for our preferred Zener model  
 488 is shown in Figure 14. The inferred coseismic potency is  $3.0 \times 10^9$  m<sup>3</sup>, equivalent to a Mw7.26  
 489 earthquake, and most of the slip is shallow and on the Sierra Cucapah fault segment. The po-  
 490 tency of five years of afterslip is  $1.1 \times 10^9$  m<sup>3</sup>. Most of the afterslip in our preferred model  
 491 occurs within the first year after the earthquake and coincides with the location of our inferred  
 492 coseismic slip. Inferred afterslip within the first year is accounting for the most rapid near-  
 493 field transient deformation. After one year, afterslip is inferred to be deeper down on the Sierra  
 494 Cucapah segment, which is describing much of the sustained near-field postseismic deforma-  
 495 tion. We emphasize, that the GPS station closest to where we infer afterslip, P496, is still about  
 496 30 km away, which is too far for us to conclusively argue for sustained localized deformation  
 497 rather than shallow distributed deformation. The deep afterslip inferred after one year could  
 498 potentially be describing deformation resulting from lower crustal flow. To test this, we have  
 499 modified our preferred model by decreasing the lower crustal viscosity from  $5.91 \times 10^{19}$  Pa



473 **Figure 12.** Mean chi-squared value for the best fitting slip model as a function of the transient shear modu-  
 474 lus relative to the elastic shear modulus in a Zener upper mantle. Large dot indicates our preferred ratio.



475 **Figure 13.** Observed postseismic displacements (black). Predicted postseismic displacements for the best  
 476 fitting slip model when assuming a Maxwell viscoelastic lower crust and upper mantle (blue). Predicted post-  
 477 seismic displacements for the best fitting slip model when assuming a Maxwell viscoelastic lower crust and a  
 478 Zener viscoelastic upper mantle (green). The effective viscosities are the same for both models and are shown  
 479 in Figure 10.



522 **Figure 14.** Inferred coseismic slip and afterslip when assuming a Maxwell rheology in the lower crust and  
 523 a Zener rheology in the upper mantle. The transient viscosity  $\eta_K$  in the mantle and steady-state viscosity  $\eta_M$   
 524 in the crust are set equal to the effective viscosities from Figure 10. We set  $\frac{\mu_K}{\mu} = 0.375$  in the upper mantle.

500 s to  $1 \times 10^{19}$  Pa s, which is still consistent with our viscosity inference from Section 3.2, and  
 501 inverted for fault slip. We find that a model with a weaker lower crust adequately describes  
 502 the postseismic displacements without any afterslip after one year, while still requiring about  
 503 the same amount of afterslip over the first year. We do believe that the early shallow afterslip  
 504 on the Sierra Cucapah segment is a robust feature in our preferred model, while we are not  
 505 confident in our inference of later deep afterslip.

506 the postseismic displacements predicted by our preferred model are shown in Figures  
 507 3, 4 and 13. Overall, the trends in the near-field and far-field transient deformation are accu-  
 508 rately described. In particular, the trends in far-field deformation are much better described  
 509 by our preferred Zener model than either an elastic model or a model with a Maxwell viscoelas-  
 510 tic mantle (Figure 13). There are a few areas where we have notable misfit. Most of our mis-  
 511 fit is for the near-field stations in the Imperial Valley, and we attribute this misfit to our rel-  
 512 atively simple fault geometry, which does not account for potential fault slip in the Imperial  
 513 Valley triggered by the El Mayor-Cucapah earthquake [Wei *et al.*, 2011a, 2015]. In particu-  
 514 lar, we are unable to model the sustained, rapid rate of deformation at station P496, which sug-  
 515 gests that this station could be influenced by a more localized deformation mechanism than  
 516 is considered in this study. Additionally, we see systematic misfit in the later postseismic pe-  
 517 riod west of the Landers and Hector Mine earthquakes, which may be the result of unmod-  
 518 eled postseismic deformation resulting from those earthquakes. Lastly, there are clear discrep-  
 519 ancies between the observed and predicted vertical deformation following the first year after  
 520 the El Mayor Cucapah earthquake. We observe a broad uplift throughout Southern Califor-  
 521 nia, which is inconsistent with any postseismic model.

## 525 4 Discussion

526 It has long been recognized that deep afterslip and viscoelastic relaxation following an  
 527 upper crustal earthquake can result in similar horizontal ground deformation at the surface [e.g.  
 528 Savage, 1990; Pollitz *et al.*, 2001; Hearn, 2003; Feigl and Thatcher, 2006]. The similarity of  
 529 the horizontal postseismic deformation results in a non-uniqueness in inferences of afterslip  
 530 or viscoelastic relaxation. In contrast, the spatial pattern of vertical postseismic deformation  
 531 has been proposed to be a discriminant between deep afterslip and viscoelastic relaxation [e.g.

532 *Pollitz et al.*, 2001; *Hearn*, 2003]. It is, however, important to note that patterns of vertical de-  
 533 formation are very sensitive to the depth-dependence of viscosity below the upper crust [Yang  
 534 and Toksöz, 1981; *Hetland and Zhang*, 2014]. The similarity between deformation resulting  
 535 from deep afterslip and viscoelastic relaxation of coseismic stresses is different from the ill-  
 536 posedness described in Section 3.2. In our method, any inferred afterslip will also mechani-  
 537 cally drive additional viscoelastic relaxation. The horizontal deformation resulting from deep  
 538 afterslip will generally be in the opposite direction as horizontal deformation resulting from  
 539 viscoelastic relaxation of subsequent stresses in the lower crust (Figure 8). As a result, there  
 540 is a trade-off between inferences of deep afterslip and lower crustal viscosity. In our synthetic  
 541 tests in *Hines and Hetland* [2016], we have found that inverting surface deformation for af-  
 542 terslip and viscosity within the same depth interval tends to result in overestimated afterslip  
 543 and an underestimated viscosity.

544 Most postseismic studies assume Maxwell viscoelasticity in the lower crust and upper  
 545 mantle [e.g. *Nur and Mavko*, 1974; *Pollitz et al.*, 2000; *Hetland*, 2003; *Freed et al.*, 2006; *John-*  
 546 *son et al.*, 2009; *Hearn et al.*, 2009], which is the simplest viscoelastic rheologic model. In South-  
 547 ern California, postseismic studies following the Landers [*Pollitz et al.*, 2000], Hector Mine  
 548 [*Pollitz et al.*, 2001], and El Mayor-Cucapah earthquake [*Spinler et al.*, 2015; *Rollins et al.*, 2015],  
 549 have assumed Maxwell viscoelasticity in the lower crust and upper mantle and have inferred  
 550 upper mantle viscosities on the order of  $10^{17}$  to  $10^{18}$  Pa s and lower crust viscosities  $\gtrsim 10^{19}$   
 551 Pa s. These postseismic studies are consistent with *Kaufmann and Amelung* [2000] and *Cava-*  
 552 *alié et al.* [2007], who found that an upper mantle viscosity of  $10^{18}$  Pa s and a crustal viscos-  
 553 ity  $\gtrsim 10^{20}$  Pa s are necessary to describe subsidence resulting from changes in loading from  
 554 Lake Mead. This isostatic adjustment is a process with similar spatial and temporal scales as  
 555 postseismic deformation, and thus the inferred viscosities of these two types of studies would  
 556 likely agree. While these studies found viscosities that are consistent with our effective vis-  
 557 cosities from Section 3.2, they are inconsistent with viscosity estimates made from geophys-  
 558 ical processes that occur over longer time scales. For example, *Lundgren et al.* [2009] found  
 559 that lower crust and upper mantle viscosities on the order of  $10^{21}$  and  $10^{19}$  Pa s, respectively,  
 560 are needed to describe interseismic deformation along the Southern San Andreas fault zone  
 561 in the Salton Sea region. An even higher mantle viscosity, on the order of  $10^{20}$  Pa s, is re-  
 562 quired to describe isostatic adjustment resulting from the draining of Lake Bonneville, which  
 563 occurs on the time scales of  $10^4$  years [*Crittenden*, 1967; *Bills and May*, 1987].

564 An additional deficiency with the Maxwell rheology is that it predicts a steady decay  
 565 in the rate of postseismic deformation over time, which fails to describe the commonly ob-  
 566 served rapid, early transience followed by a relatively steady rate of postseismic deformation.  
 567 One could explain the early transient postseismic deformation with fault creep and the later  
 568 phase with relaxation in a Maxwell viscoelastic lower crust and upper mantle [e.g. *Hearn et al.*,  
 569 *Johnson et al.*, 2009]. However, postseismic deformation at distances greater than  $\sim 200$   
 570 km from the El Mayor-Cucapah epicenter can only be attributed to viscoelastic relaxation [*Freed*  
 571 *et al.*, 2007] and we have demonstrated that the far-field deformation cannot be explained with  
 572 a Maxwell rheology (Figure 13).

573 We found that a Zener rheology in the upper mantle with a transient viscosity of  $\sim 10^{18}$   
 574 Pa s does a noticeably better job at predicting far-field postseismic deformation. A general-  
 575 ization of the Zener viscoelastic model, schematically represented as several Kelvin elements  
 576 connected in series, is commonly used to describe seismic attenuation [*Liu et al.*, 1976]. The  
 577 highest viscosity needed to describe seismic attenuation is on the order of  $10^{16}$  Pa s [*Yuen and*  
 578 *Peltier*, 1982] which has a characteristic relaxation time on the order of days. Even though  
 579 our inferred transient viscosity is orders of magnitude larger than that required for seismic at-  
 580 tenuation models, the two models are not incompatible. Rather, the delayed elasticity in seis-  
 581 mic attenuation models occurs on such short time scales that it can be considered part of the  
 582 instantaneous elastic phase of deformation associated with the preferred Zener model in this  
 583 study.

584 Of course, it has long been recognized that a Zener rheology provides an incomplete de-  
 585 scriptions of the asthenosphere, as it does not have the fluid-like behavior required to explain  
 586 isostatic rebound or convection in the mantle [O'Connell, 1971]. Yuen and Peltier [1982] pro-  
 587 posed a Burgers rheology with a low transient viscosity ( $\eta_K \approx 10^{16}$  Pa s) and high steady-  
 588 state viscosity ( $\eta_M \approx 10^{21}$  Pa s) to describe both seismic attenuation and long term geologic  
 589 processes. The justification of a Burger's rheology mantle is further supported by laboratory  
 590 experiments on olivine [Chopra, 1997]. Pollitz [2003] sought to describe postseismic defor-  
 591 mation following Hector Mine with a Burgers rheology mantle and they found a best fitting  
 592 transient viscosity of  $1.6 \times 10^{17}$  Pa s and steady-state viscosity of  $4.6 \times 10^{18}$  Pa s. While  
 593 the Burgers rheology was introduced as a means of bridging the gap between relaxation ob-  
 594 served in long and short term geophysical processes, the inferred steady state viscosity from  
 595 Pollitz [2003] is still inconsistent with the Maxwell viscosities inferred from studies on the earth-  
 596 quake cycle and Lake Bonneville. The transient viscosity inferred by Pollitz [2003] is constrained  
 597 by the earliest phase of postseismic deformation following the Hector Mine earthquake. While  
 598 Pollitz [2003] ruled out deep afterslip as an alternative mechanism based on inconsistent ver-  
 599 tical deformation, it is still possible to successfully describe all components of early postseis-  
 600 mic deformation following the Hector Mine earthquake with afterslip at seismogenic depths  
 601 [Jacobs et al., 2002]. It is then possible that the preferred rheologic model from Pollitz [2003]  
 602 was biased towards inferring a particularly low transient viscosity by neglecting to account for  
 603 afterslip. This is in contrast to the present study, where we have inferred a viscosity structure  
 604 simultaneously with afterslip. We also argue that a transient rheology is necessary to explain  
 605 postseismic deformation; however, our preferred transient viscosity of  $\sim 10^{18}$  Pa s in the up-  
 606 per mantle is an order of magnitude larger than the transient viscosity found by Pollitz [2003].  
 607 Since a Zener model is able to describe the available postseismic deformation following the  
 608 El Mayor-Cucapah earthquake, any Burgers rheology with a steady-state viscosity that is  $\gtrsim$   
 609  $10^{20}$  Pa s, effectively infinite over five years, would also be able to describe the postseismic  
 610 deformation. Such a Burgers model might then be consistent with the steady-state viscosities  
 611 necessary for lake loading, interseismic deformation, and mantle dynamics.

## 612 5 Conclusion

613 We have extracted a filtered and smoothed estimate of postseismic deformation follow-  
 614 ing the El Mayor-Cucapah earthquake from GPS displacement time series. We treated post-  
 615 seismic deformation as a stochastic process where we did not presume any characteristic shape  
 616 of the postseismic time series. Our estimated postseismic deformation reveals far-field (epi-  
 617 central distances beyond  $\sim 200$  km) transient deformation which is largely undetectable after  
 618 about three years. Near-field deformation exhibits transience that decays to a sustained, ele-  
 619 vated rate after about one or two years. We found that near-field transient deformation can be  
 620 explained with shallow afterslip, and the sustained rate of near-field deformation can either  
 621 be explained with continued afterslip or relaxation in a lower crustal with a viscosity of  $\sim 10^{19}$   
 622 Pa s. Far-field transient deformation can be more definitively ascribed to viscoelastic relax-  
 623 ation at depths greater than  $\sim 60$  km. Beneath that depth, a transient viscosity of  $\sim 10^{18}$  Pa s  
 624 is required to describe the rate of far-field deformation throughout the five years considered  
 625 in this study. By describing the available postseismic deformation with a transient rheology  
 626 in the mantle, our preferred model does not conflict with the generally higher steady-state vis-  
 627 cosities inferred from geophysical processes occurring over longer time scales.

## 628 Acknowledgements

629 We thank Andy Freed for an illuminating discussion on the data used in this study. This  
 630 material is based on EarthScope Plate Boundary Observatory data services provided by UN-  
 631 AVCO through the GAGE Facility with support from the National Science Foundation (NSF)  
 632 and National Aeronautics and Space Administration (NASA) under NSF Cooperative Agree-  
 633 ment No. EAR-1261833. The data used in this study can be found at [www.unavco.org](http://www.unavco.org). This

634 material is based upon work supported by the National Science Foundation under Grant Num-  
 635 bers EAR 1045372 and EAR 1245263.

## 636 References

- 637 Aagaard, B. T., M. G. Knepley, and C. A. Williams (2013), A domain decomposition  
 638 approach to implementing fault slip in finite-element models of quasi-static and dy-  
 639 namic crustal deformation, *Journal of Geophysical Research: Solid Earth*, 118, doi:  
 640 10.1002/jgrb.50217.
- 641 Argus, D. F., M. B. Heflin, G. Peltzer, F. Crampé, and F. H. Webb (2005), Interseismic  
 642 strain accumulation and anthropogenic motion in metropolitan Los Angeles, *Journal of*  
 643 *Geophysical Research: Solid Earth*, 110(4), 1–26, doi:10.1029/2003JB002934.
- 644 Aster, R. C., B. Borchers, and C. H. Thurber (2011), Parameter Estimation and Inverse  
 645 Problems, vol. 90, Academic Press.
- 646 Bawden, G. W., W. Thatcher, R. S. Stein, K. W. Hudnut, and G. Peltzer (2001), Tectonic  
 647 contraction across Los Angeles after removal of groundwater pumping effects., *Nature*,  
 648 412(August), 812–815, doi:10.1038/35090558.
- 649 Bills, B. G., and G. M. May (1987), Lake Bonneville: Constraints on Lithospheric Thick-  
 650 ness and Upper Mantle Viscosity From Isostatic Warping of Bonneville, Provo, and  
 651 Gilbert Stage Shorelines, *Journal of Geophysical Research-Solid Earth and Planets*,  
 652 92(B11), 11,493–11,508, doi:10.1029/JB092iB11p11493.
- 653 Çakir, Z., S. Ergintav, H. Özener, U. Dogan, A. M. Akoglu, M. Meghraoui, and  
 654 R. Reilinger (2012), Onset of aseismic creep on major strike-slip faults, *Geology*,  
 655 40(12), 1115–1118, doi:10.1130/G33522.1.
- 656 Cavalié, O., M. P. Doin, C. Lasserre, and P. Briole (2007), Ground motion measurement in  
 657 the Lake Mead area, Nevada, by differential synthetic aperture radar interferometry time  
 658 series analysis: Probing the lithosphere rheological structure, *Journal of Geophysical*  
 659 *Research: Solid Earth*, 112(3), 1–18, doi:10.1029/2006JB004344.
- 660 Cetin, E., Z. Çakir, M. Meghraoui, S. Ergintav, and A. M. Akoglu (2014), Extent and  
 661 distribution of aseismic slip on the İsmetpaşa segment of the North Anatolian Fault  
 662 (Turkey) from Persistent Scatterer InSAR, *Geochemistry, Geophysics, Geosystems*, 15,  
 663 doi:10.1002/2014GC005307. Received.
- 664 Chopra, P. N. (1997), High-temperature transient creep in olivine rocks, *Tectonophysics*,  
 665 279, 93–111, doi:10.1016/S0040-1951(97)00134-0.
- 666 Crittenden, M. (1967), Viscosity and Finite Strength of the Mantle as Determined from  
 667 Water and Ice Loads\*, *Geophysical Journal of the Royal Astronomical ...*, pp. 261–279,  
 668 doi:10.1111/j.1365-246X.1967.tb06243.x.
- 669 Davis, J. L., B. P. Wernicke, and M. E. Tamisiea (2012), On seasonal signals in geode-  
 670 tic time series, *Journal of Geophysical Research: Solid Earth*, 117(1), 1–10, doi:  
 671 10.1029/2011JB008690.
- 672 Feigl, K. L., and W. Thatcher (2006), Geodetic observations of post-seismic transients in  
 673 the context of the earthquake deformation cycle, *Comptes Rendus - Geoscience*, 338,  
 674 1012–1028, doi:10.1016/j.crte.2006.06.006.
- 675 Fletcher, J. M., O. J. Teran, T. K. Rockwell, M. E. Osokin, K. W. Hudnut, K. J. Mueller,  
 676 R. M. Spelz, S. O. Akciz, E. Masana, G. Faneros, E. J. Fielding, S. Leprince, A. E.  
 677 Morelan, J. Stock, D. K. Lynch, A. J. Elliott, P. Gold, J. Liu-Zeng, A. González-  
 678 Ortega, A. Hinojosa-Corona, and J. González-García (2014), Assembly of a large  
 679 earthquake from a complex fault system: Surface rupture kinematics of the 4 April  
 680 2010 El Mayor-Cucapah (Mexico) Mw 7.2 earthquake, *Geosphere*, 10(4), 797–827,  
 681 doi:10.1130/GES00933.1.
- 682 Freed, A. M., R. Bürgmann, E. Calais, J. Freymueller, and S. Hreinsdóttir (2006), Impli-  
 683 cations of deformation following the 2002 Denali, Alaska, earthquake for postseismic  
 684 relaxation processes and lithospheric rheology, *Journal of Geophysical Research: Solid*  
 685 *Earth*, 111, 1–23, doi:10.1029/2005JB003894.

- 686 Freed, A. M., R. Bürgmann, and T. Herring (2007), Far-reaching transient motions after  
 687 Mojave earthquakes require broad mantle flow beneath a strong crust, *Geophysical*  
 688 *Research Letters*, *34*, 1–5, doi:10.1029/2007GL030959.
- 689 Gonzalez-Ortega, A., Y. Fialko, D. Sandwell, F. A. Nava-pichardo, J. Fletcher,  
 690 J. Gonzalez-garcia, B. Lipovsky, M. Floyd, and G. Funning (2014), El Mayor-  
 691 Cucapah (Mw7.2) earthquake: early near-field postseismic deformation from In-  
 692 Sar and GPS observations, *Journal of Geophysical Research*, *119*, 1482–1497, doi:  
 693 10.1002/2013JB010193.Received.
- 694 Hauksson, E., J. Stock, K. Hutton, W. Yang, J. A. Vidal-Villegas, and H. Kanamori  
 695 (2011), The 2010 Mw 7.2 El mayor-cucapah earthquake sequence, Baja Califor-  
 696 nia, Mexico and Southernmost California, USA: Active seismotectonics along the  
 697 Mexican pacific margin, *Pure and Applied Geophysics*, *168*(3918), 1255–1277, doi:  
 698 10.1007/s00024-010-0209-7.
- 699 Hearn, E. H. (2003), What can GPS data tell us about the dynamics of post-seismic defor-  
 700 mation ?, (2003), 753–777.
- 701 Hearn, E. H., S. McClusky, S. Ergintav, and R. E. Reilinger (2009), Izmit earthquake post-  
 702 seismic deformation and dynamics of the North Anatolian Fault Zone, *Journal of Geo-*  
 703 *physical Research: Solid Earth*, *114*(August 2008), 1–21, doi:10.1029/2008JB006026.
- 704 Hetland, E. A. (2003), Postseismic relaxation across the Central Nevada Seismic Belt,  
 705 *Journal of Geophysical Research*, *108*(Figure 2), 1–13, doi:10.1029/2002JB002257.
- 706 Hetland, E. A., and G. Zhang (2014), Effect of shear zones on post-seismic deformation  
 707 with application to the 1997 Mw 7.6 manyi earthquake, *Geophysical Journal Interna-*  
 708 *tional*, *198*, 259–269, doi:10.1093/gji/ggu127.
- 709 Hines, T. T., and E. A. Hetland (2013), Bias in estimates of lithosphere viscosity from  
 710 interseismic deformation, *Geophysical Research Letters*, *40*(16), 4260–4265, doi:  
 711 10.1002/grl.50839.
- 712 Hines, T. T., and E. A. Hetland (2016), Rapid and simultaneous estimation of fault slip  
 713 and heterogeneous lithospheric viscosity from post-seismic deformation, *Geophysical*  
 714 *Journal International*, *204*(1), 569–582, doi:10.1093/gji/ggv477.
- 715 Jacobs, A., D. Sandwell, Y. Fialko, and L. Sichoux (2002), The 1999 (Mw7.1) Hector  
 716 Mine, California, Earthquake: Near-Field Postseismic Deformation from ERS Interfer-  
 717 ometry, *Bulletin of the Seismological Society of America*, *92*(May), 1433–1442.
- 718 Johnson, K. M., and P. Segall (2004), Viscoelastic earthquake cycle models with deep  
 719 stress-driven creep along the San Andreas fault system, *Journal of Geophysical Research*  
 720 *B: Solid Earth*, *109*, 1–19, doi:10.1029/2004JB003096.
- 721 Johnson, K. M., R. Bürgmann, and J. T. Freymueller (2009), Coupled afterslip and vis-  
 722 coelastic flow following the 2002 Denali Fault, Alaska earthquake, *Geophysical Journal*  
 723 *International*, *176*(3), 670–682, doi:10.1111/j.1365-246X.2008.04029.x.
- 724 Jónsson, S., P. Segall, R. Pedersen, and G. Bjornsson (2003), Post-earthquake ground  
 725 movements correlated to pore-pressure transients, *Nature*, *424*(July), 179–183, doi:  
 726 10.1038/nature01758.1.
- 727 Kaufmann, G., and F. Amelung (2000), Reservoir-induced deformation and continental  
 728 rheology in vicinity of Lake Mead, Nevada, *Journal of Geophysical Research*, *105*(B7),  
 729 16,341, doi:10.1029/2000JB900079.
- 730 Kroll, K. A., E. S. Cochran, K. B. Richards-Dinger, and D. F. Sumy (2013), Aftershocks  
 731 of the 2010 Mw 7.2 El Mayor-Cucapah earthquake reveal complex faulting in the Yuha  
 732 Desert, California, *Journal of Geophysical Research: Solid Earth*, *118*(October), 6146–  
 733 6164, doi:10.1002/2013JB010529.
- 734 Lekic, V., S. W. French, and K. M. Fischer (2011), Lithospheric Thinning Beneath Rifted  
 735 Regions of Southern California, *Science*, *334*(November), 783–787.
- 736 Liu, H.-P., D. L. Anderson, and H. Kanamori (1976), Velocity dispersion due to anelastic-  
 737 ity; implications for seismology and mantle composition, *Geophysical Journal Interna-*  
 738 *tional*, *47*(1), 41–58, doi:10.1111/j.1365-246X.1976.tb01261.x.

- Lundgren, P., E. A. Hetland, Z. Liu, and E. J. Fielding (2009), Southern San Andreas-San Jacinto fault system slip rates estimated from earthquake cycle models constrained by GPS and interferometric synthetic aperture radar observations, *Journal of Geophysical Research: Solid Earth*, **114**(2), 1–18, doi:10.1029/2008JB005996.
- McGuire, J. J., and P. Segall (2003), Imaging of aseismic fault slip transients recorded by dense geodetic networks, *Geophysical Journal International*, **155**(3), 778–788, doi: 10.1111/j.1365-246X.2003.02022.x.
- Meade, B. J., and B. H. Hager (2005), Block models of crustal motion in southern California constrained by GPS measurements, *Journal of Geophysical Research B: Solid Earth*, **110**, 1–19, doi:10.1029/2004JB003209.
- Murray, J. R., and P. Segall (2005), Spatiotemporal evolution of a transient slip event on the San Andreas fault near Parkfield, California, *Journal of Geophysical Research : Solid Earth*, **110**(9), 1–12, doi:10.1029/2005JB003651.
- Nur, A., and G. Mavko (1974), Postseismic viscoelastic rebound, *Science*, **183**(4121), 204–206, doi:10.1038/098448b0.
- O'Connell, R. J. (1971), Rheology of the Mantle, *EOS, Transactions, American Geophysical Union*, **52**, 140–142.
- Oskin, M. E., J. R. Arrowsmith, A. Hinojosa Corona, A. J. Elliott, J. M. Fletcher, E. J. Fielding, P. O. Gold, J. J. Gonzalez Garcia, K. W. Hudnut, J. Liu-Zeng, and O. J. Teran (2012), Near-field deformation from the El Mayor-Cucapah earthquake revealed by differential LIDAR, *Science*, **335**(6069), 702–705, doi:10.1126/science.1213778.
- Pollitz, F., C. Wicks, and W. Thatcher (2001), Mantle Flow Beneath a Continental Strike-Slip Fault : Postseismic Deformation After the 1999 Hector Mine Earthquake, *Science*, **1814**(2001), 1814–1818, doi:10.1126/science.1061361.
- Pollitz, F. F. (2003), Transient rheology of the uppermost mantle beneath the Mojave Desert, California, *Earth and Planetary Science Letters*, **215**, 89–104, doi: 10.1016/S0012-821X(03)00432-1.
- Pollitz, F. F., G. Peltzer, and R. Bürgmann (2000), Mobility of continental mantle: Evidence from postseismic geodetic observations following the 1992 Landers earthquake, *Journal of Geophysical Research*, **105**(1999), 8035, doi:10.1029/1999JB900380.
- Pollitz, F. F., R. Bürgmann, and W. Thatcher (2012), Illumination of rheological mantle heterogeneity by the M7.2 2010 El Mayor-Cucapah earthquake, *Geochemistry, Geophysics, Geosystems*, **13**(6), 1–17, doi:10.1029/2012GC004139.
- Rauch, H. E., F. Tung, and C. T. Striebel (1965), Maximum likelihood estimates of linear dynamic systems, *AIAA Journal*, **3**(8), 1445–1450.
- Riva, R. E. M., and R. Govers (2009), Relating viscosities from postseismic relaxation to a realistic viscosity structure for the lithosphere, *Geophysical Journal International*, **176**, 614–624, doi:10.1111/j.1365-246X.2008.04004.x.
- Rollins, C., S. Barbot, and J.-P. Avouac (2015), Postseismic Deformation Following the 2010 M7.2 El Mayor-Cucapah Earthquake : Observations , Kinematic Inversions , and Dynamic Models, *Pure and Applied Geophysics*, doi:10.1007/s00024-014-1005-6.
- Savage, J. C. (1990), Equivalent strike-slip earthquake cycles in half-space and lithosphere-asthenosphere earth models, *Journal of Geophysical Research*, **95**, 4873, doi:10.1029/JB095iB04p04873.
- Savage, J. C., and J. L. Svare (2009), Postseismic relaxation following the 1992 M 7.3 Landers and 1999 M 7.1 Hector Mine earthquakes , southern California, *Journal of Geophysical Research*, **114**(B01401), doi:10.1029/2008JB005938.
- Savage, J. C., J. L. Svare, and S. B. Yu (2005), Postseismic relaxation and transient creep, *Journal of Geophysical Research: Solid Earth*, **110**, 1–14, doi:10.1029/2005JB003687.
- Segall, P., and M. Mathews (1997), Time dependent inversion of geodetic data, *Journal of Geophysical Research*, **102**.
- Spinler, J. C., R. A. Bennett, C. Walls, L. Shawn, and J. J. G. Garcia (2015), Assessing long-term postseismic deformation following the M7.2 4 April 2010, El Mayor-Cucapah earthquake with implications for lithospheric rheology in the

- 793 Salton Trough, *Journal of Geophysical Research: Solid Earth*, 120, 3664–3679, doi:  
794 10.1002/2014JB011613.Received.
- 795 Wei, M., D. Sandwell, Y. Fialko, and R. Bilham (2011a), Slip on faults in the Imperial  
796 Valley triggered by the 4 April 2010 Mw 7.2 El Mayor-Cucapah earthquake revealed by  
797 InSAR, *Geophysical Research Letters*, 38(January), 1–6, doi:10.1029/2010GL045235.
- 798 Wei, M., Y. Liu, Y. Kaneko, J. J. McGuire, and R. Bilham (2015), Dynamic triggering of  
799 creep events in the Salton Trough, Southern California by regional M5.4 earthquakes  
800 constrained by geodetic observations and numerical simulations, *Earth and Planetary  
Science Letters*, 427, 1–10, doi:10.1016/j.epsl.2015.06.044.
- 801 Wei, S., E. Fielding, S. Leprince, A. Sladen, J.-P. Avouac, D. Helmberger, E. Hauksson,  
802 R. Chu, M. Simons, K. Hudnut, T. Herring, and R. Briggs (2011b), Superficial sim-  
803 plicity of the 2010 El MayorCucapah earthquake of Baja California in Mexico, *Nature  
Geoscience*, 4(9), 615–618, doi:10.1038/ngeo1213.
- 804 Yang M., and M. N. Toksöz (1981), Time-dependent deformation and stress relaxation  
805 after strike-slip earthquakes, *Journal of Geophysical Research*, 86, 2889–2901.
- 806 Yuen, D. A., and W. R. Peltier (1982), Normal modes of the viscoelastic earth, *Geo-  
807 physical Journal of the Royal Astronomical Society*, 69, 495–526, doi:10.1111/j.1365-  
808 246X.1982.tb04962.x.
- 810